SNARE-mediated membrane fusion trajectories derived from force-clamp experiments

Marieelen Oelkers[a,1], Hannes Witt[a,1], Partho Halder[b], Reinhard Jahn[b], and Andreas Janshoff[a,2]

[a]Institute of Physical Chemistry, University of Göttingen, 37077 Goettingen, Germany; and [b]Department of Neurobiology, Max Planck Institute for Biophysical Chemistry, 37077 Goettingen, Germany

Edited by Taekjip Ha, Johns Hopkins University, Baltimore, MD, and approved October 12, 2016 (received for review September 27, 2016)

Fusion of lipid bilayers is usually prevented by large energy barriers arising from removal of the hydration shell, formation of highly curved structures, and, eventually, fusion pore widening. Here, we measured the force-dependent lifetime of fusion intermediates using membrane-coated silica spheres attached to cantilevers of an atomic-force microscope. Analysis of time traces obtained from force-clamp experiments allowed us to unequivocally assign steps in deflection of the cantilever to membrane states during the SNARE-mediated fusion with solid-supported lipid bilayers. Force-dependent lifetime distributions of the various intermediate fusion states allowed us to propose the likelihood of different fusion pathways and to assess the main free energy barrier, which was found to be related to passing of the hydration barrier and splaying of lipids to eventually enter either the fully fused state or a long-lived hemifusion intermediate. The results were compared with SNARE mutants that arrest adjacent bilayers in the docked state and membranes in the absence of SNAREs but presence of PEG or calcium. Only with the WT SNARE construct was appreciable merging of both bilayers observed.

membrane fusion | SNARE | force spectroscopy | AFM | hydration barrier

Membrane fusion plays a pivotal role in many fundamental biological processes, comprising viral infection, cell–cell fusion during fertilization, tissue formation, and intracellular transport during exo- and endocytosis (1). Among the best-studied biological examples is the Ca^{2+}-regulated fusion of synaptic vesicles with the presynaptic plasma membrane in neurons and chromaffin cells (2, 3). Fusion in these cells is catalyzed by concerted action of SNARE proteins through formation of a tetrameric coiled-coil complex that releases a sufficient amount of free energy to lower the barriers for membrane merging. One major energy barrier is associated with the strong repulsive hydration forces when two smooth bilayers approach each other. Other energy-costly contributions originate from lipid splaying as the initiation of stalk formation, expansion of the stalk structure driven by the strong curvature associated with membrane destabilization, hemifusion diaphragm expansion, and, finally, pore formation (4–8). The free energy associated with complex formation and folding of SNAREs was reported to be ∼35 k_BT, close to the energy required to create the highly curved transition structures (40–50 k_BT) (9, 10). Albeit a part of this free energy might be dissipated as heat, this coincidence of matching energy is also supported by experimental studies showing that only very few SNARE complexes are sufficient to induce fusion in artificial systems (5, 6, 11–13). Although precise data for thermodynamics and kinetics of SNARE zippering and unzippering are now available (11, 14, 15), few studies address how the energy landscape of membrane fusion is shaped by participation of SNAREs. Israelachvili and coworkers (16–18) were among the first to measure fusion events in the absence of proteins as a function of external force using a surface force apparatus, and Moy and coworkers (19) measured the interaction forces between reconstituted SNARE derivatives, reporting fusion events as mechanical instabilities in the approach curve of the two membrane-coated substrates. Additional advances have been made by Brouwer et al. (20) and Keidel et al. (21) by using optical tweezers for studying some aspects of membrane fusion.

Here, we used membrane-coated colloidal probes in contact with solid-supported membranes to monitor fusion catalyzed by SNAREs as a function of externally applied pressure. We found that formation of the SNARE complex, stalk formation, hemifusion, and full fusion can be distinguished and that it is possible to precisely reconstruct fusion trajectories and the basic energy landscape by measuring lifetime distributions of intermediate states as a function of elastic energy added to the system. Essentially, we found that all energy barriers are substantially lowered due to the presence of SNAREs, but the barrier associated with removal of the hydration shell remains the most prominent one.

Results

A label-free technique based on colloidal probe microscopy with membrane-coated beads, which permits one to study fusion events and the lifetime of their intermediate states with subnanometer and millisecond resolution (Fig. 1*A*), has been devised. We used a stabilized SNARE acceptor complex consisting of syntaxin 1, SNAP-25, and a C-terminal fragment of synaptobrevin (referred to as ΔN-acceptor complex) that was shown previously to mediate rapid fusion with synaptobrevin-containing liposomes (22). Two opposing bilayers equipped with synaptobrevin and the ΔN-acceptor were separately deposited via vesicle spreading on a silica bead attached to a tipless cantilever (red) and on a glassy surface (green), respectively (Fig. 1*A*). The experiment is conducted as follows (Fig. 1*B*). Two bilayers are quickly brought into contact until a defined force is reached. Once the yield force is reached the force feedback of the atomic-force microscope (AFM) is switched off and the cantilever deflection monitored as a function of time at a noise level of 0.5 nm (rms). In the presence of SNAREs, we frequently found that cantilever deflection stochastically jumps within milliseconds several nanometers

Significance

Fusion of membranes plays an important role in many biological processes such as vesicle trafficking and viral infection. However, without assistance from specialized proteins such as SNAREs the energy barriers associated with merging of two bilayers are too high to achieve fast kinetics as required for the release of neurotransmitters. We devised a method based on colloidal probe microscopy that allows monitoring the distance of two membranes at a defined contact pressure, providing access to the lifetime of intermediate states of fusion. Changing the contact pressure gives access to the energy landscape and kinetic rates of fusion in the presence of neuronal SNARE proteins. This allows one to explore fusion pathways as a function of molecular composition and environmental cues.

Author contributions: R.J. and A.J. designed research; M.O., H.W., and P.H. performed research; and M.O., H.W., and A.J. wrote the paper.

The authors declare no conflict of interest.

This article is a PNAS Direct Submission.

[1]M.O. and H.W. contributed equally to this work.

[2]To whom correspondence should be addressed. Email: ajansho@gwdg.de.

This article contains supporting information online at www.pnas.org/lookup/suppl/doi:10.1073/pnas.1615885113/-/DCSupplemental.

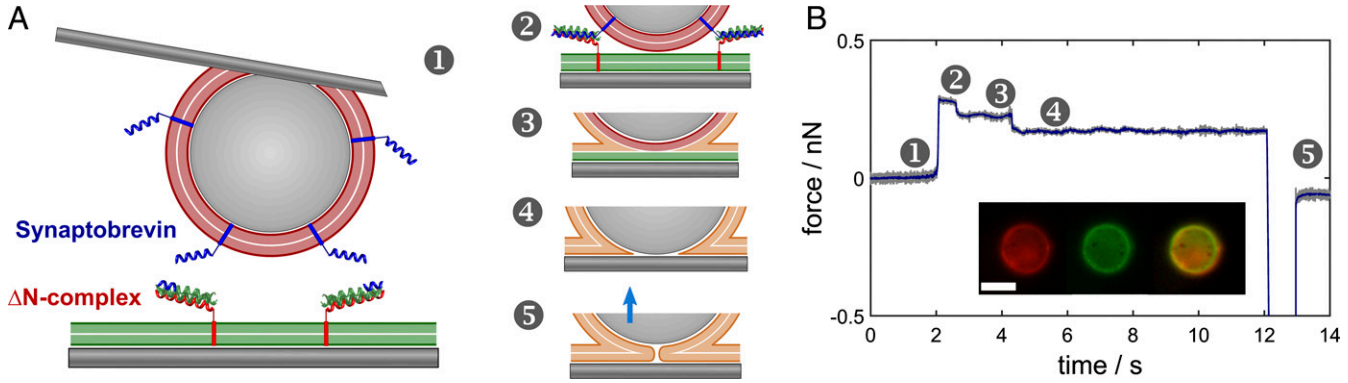

Fig. 1. (*A*) A micrometer-sized silica sphere is covered with a lipid bilayer (red) equipped with synaptobrevin (syb) and brought into contact with a solid-supported bilayer (green) on silica functionalized with the ΔN-complex. The following discrete states are distinguished: (1) free probe, docking in contact (2), followed by hemifusion (3) and, eventually, full merging of the two bilayers (4). Desorption from the surface (5) reveals a large adhesion energy due to strong attractive van der Waals interactions between the two silica surfaces. (*B*) Experimental force cycle in which the aforementioned intermediates are assigned. (*Inset*) Fluorescence images of the colloidal probe after successful fusion events at the end of an experiment. Left: red channel, center: green channel, right: merging of the two channels. (Scale bar, 10 μm.)

toward the surface. After a contact time of 10 s the two surfaces are separated and the corresponding adhesion force is recorded.

Analysis of the step height distribution (Fig. 2*A*) and correlation with the corresponding adhesion forces (Fig. 2*B*) allowed us to assign the observed steps in the time traces to prominent recurrent fusion intermediates. The step height distribution could be well described by the sum of four Gaussians (Fig. 2*A*, dotted line). The most unequivocal assignments are fusion of only two leaflets (hemifusion or subsequent full fusion, 2.1–4.2 nm, blue line) and merging of outer and inner leaflets (one-step full fusion, 4.2–8.4 nm, green line), characterized by step heights corresponding to removal of a single bilayer or two bilayers, respectively. Full merging of both bilayers is associated with large adhesion forces attributed to strong van der Waals interaction between two silica surfaces. The step heights are slightly lower than expected for the thickness of unperturbed bilayers due to the external compressional force. Assuming a Hertzian contact model with a Young's modulus of 20 MPa, we estimate a reduced thickness of ∼0.25 nm at 200 pN (23, 24). Steps bigger than the height of two bilayers are probably caused by the displacement of adherent vesicles or stacked bilayer sheets (orange line). The smaller steps below 2 nm (red line) are frequently found before fusion events and are attributed to stalk formation after crossing the hydration barrier (discussed below). Taken together, we can resolve removal of the hydration shell or stalk formation through lipid splay, merging of the outer leaflets, and full fusion of both leaflets until the bead is again separated from the sample displaying adhesion forces that correlate with the preceding events (Fig. 2*B*). For each set of parameters at least 200 independent force–distance cycles were recorded.

We also successfully verified full merging of lipids by fluorescence microscopy (Fig. 1*B*, *Inset*). Before contact, the bilayer deposited on the colloidal probe was doped with a red fluorophore (Texas Red), and the opposing bilayer on the planar substrate was labeled with a green fluorophore (Oregon Green). After detecting fusion events in the time traces of cantilever deflection, lipid mixing was found in fluorescence images of the cantilever-attached bead.

Fig. 2*C* shows representative experiments in which the various steps in membrane fusion are resolved and identified. Full fusion was observed as a one-step reaction (Fig. 2*C*, *Top*) but also as two consecutive events (Fig. 2*C*, *Center*). In some time traces the system remained either in a docked (not shown) or hemifused state (Fig. 2*C*, *Bottom*). If both leaflets fuse, as indicated by a cumulative step height in a single trace larger than 4–5 nm also very large attractive forces of up to 8 nN occur due to the strong van der Waals attraction between silica surfaces (Fig. 2*B*) (25). Hemifusion with a cumulative step height between 2 and 5 nm was associated with adhesion forces around 1 nN, substantially

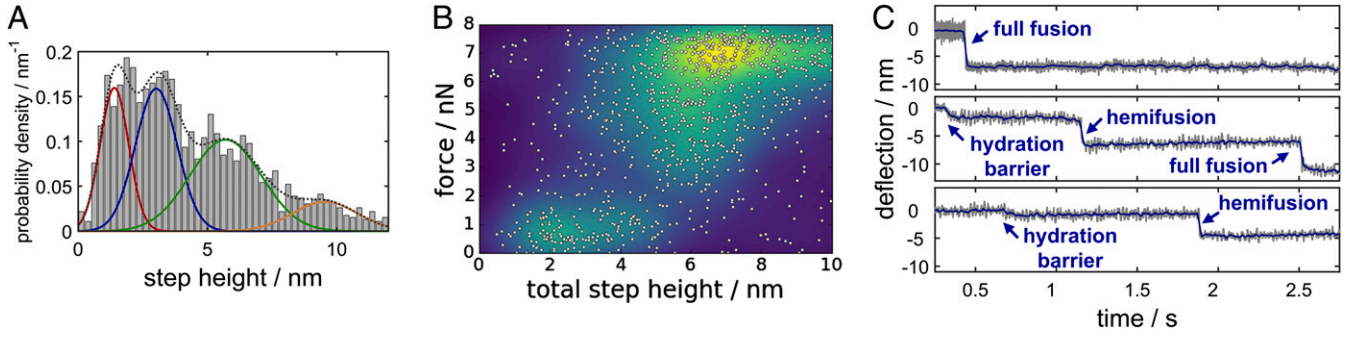

Fig. 2. (*A*) Histogram of the step heights found in time traces of force clamp experiments. We attribute the measured step height to events such as crossing of the hydration barrier (red), hemifusion corresponding to a step height of a single bilayer (blue), and full fusion indicated by a step height equivalent to the thickness of two compressed bilayers (green). The orange line indicates either crossing of multibilayers or vesicle displacement. (*B*) Adhesion force (after separating the bead from the sample) as a function of the total step height. (*C*) Representative time traces of cantilever during contact of the two membranes. Three typical scenarios are frequently observed: full merging of the two bilayers in one step (*Top*), consecutive fusion of the outer and the inner leaflets (*Center*), and a state arrested in hemifusion (*Bottom*). Frequently small steps corresponding to crossing of the hydration barrier were found ahead of fusion events (*Center* and *Bottom*).

larger than forces associated with docking. If no membrane fusion was detected as indicated by step sizes <2 nm the measured adhesion forces correspond to the unzippering forces of the SNARE or extraction of the SNAREs from the bilayer (Fig. 3*A*, *Top* and Fig. S1). We found discrete detachment events corresponding to one to five SNARE molecules each with a force maximum of 200 ± 37 pN upon separation of nonfused bilayers, in agreement with reported rupture forces for SNARE assemblies (26, 27).

We observed that once the membranes started to merge both hemifusion and full fusion occur rather quickly (1–4 ms) on time scales corresponding to lateral diffusion of lipids limited by the viscous drag of the cantilever (0.1–0.2 ms) (Fig. S2) (16–18).

The following control measurements were carried out. First, we used membrane-coated beads and planar surfaces in which either synaptobrevin was replaced by a point mutant capable of partial zippering but not (hemi)fusion (Δ84 syb) (28) or in which SNAREs were entirely absent. Second, we performed experiments in the absence of SNARE proteins with HP150 buffer doped with 6 wt % PEG-8000, which has been reported to significantly weaken hydration repulsion (29). Additionally, all experiments were carried out either in the presence or in absence of 1 mM calcium to examine its role in membrane fusion. We found that at a given compressional force of 200 pN and a contact time of 10 s merging of outer and inner leaflets occurred substantially more frequently if WT SNAREs were used in the presence of calcium ions with a probability of 24.5% (Fig. 3*B*), comprised of 22.5% one-step full fusion and only 2% full fusion with a hemifusion intermediate. Fusion occurs also with a lower but still noticeable probability of 7.6% if WT SNAREs were used in the absence of calcium ions. However, the probability for the system to remain in a hemifused state increases from 6.25% in the presence of calcium to 16.2% in the absence of calcium.

In the absence of both calcium and SNAREs the number of mechanical instabilities associated with barrier crossing is very low. In the presence of calcium but absence of SNAREs, any fusion-related events are detected mainly if the integrity of the supported bilayer was partly compromised (i.e., showing defects) (17, 18). The likelihood for membranes to cross the hydration barrier but not to merge increases strongly from 9 to 15% when PEG and calcium were added to the system, attributed to lowering of the hydration barrier. Recognition (adhesion forces larger than 50 pN) occurred with high probability as long as SNAREs—both WT and mutant—were present. Similarly, the probability of finding attractive interaction forces between the bilayers increased with the addition of PEG.

Formation of SNARE complexes was highly probable also if the Δ84 syb mutant was used instead of WT SNAREs and the frequency of complex formation did not depend on the presence of calcium ions. However, we found that the binding strength varies substantially between WT synaptobrevin and the Δ84 syb mutant in the presence and absence of calcium (Fig. 3*A*). We only selected desorption events for the analysis of single-molecule rupture forces where no fusion occurred during the contact of both bilayers to ensure that the observed adhesion originates solely from SNARE unzippering. A single WT SNARE complex displayed rupture forces of 200 ± 37 pN, whereas the Δ84 syb mutant showed only a rupture force of 120 ± 23 pN. This reduction in dynamic strength can be attributed to the fact that the mutation abolishes the last +8 layer of the SNARE complex (28). In both cases between one and five SNARE complexes were stochastically formed in the contact zone, in agreement with the expected value of two SNAREs calculated from protein density and the contact radius according to Hertz theory (23). Recognition events are also observed in the absence of calcium, but unbinding forces are greatly reduced to 70 ± 13 pN per WT SNARE complex and 60 ± 7 pN for the Δ84 syb mutant (Fig. S3). Also, the number of SNARE complexes formed is reduced to one to three SNARE complexes. We cannot entirely rule out that extraction of SNAREs upon retraction occurs, but the forces agree well with previous reports and extraction followed by unfolding would not depend that strongly on the presence of calcium or on point mutations as observed here (26, 27). Besides, constant fusion efficiency over 1,000 force–distance cycles was found, which speaks against extraction of SNAREs from the bilayer. It is conceivable that laterally formed clusters stabilize SNARE against extraction from the membrane (30).

The prime advantage of using colloidal probes attached to a force transducer is that we can apply external load in a defined manner, thereby substantially altering reaction rates. For each constant loading force we consider the average lifetime between initial contact and crossing of the hydration barrier, between crossing of the hydration barrier and hemifusion or one-step full fusion, and between hemifusion and consecutive full fusion (Fig. 4*A*). We found that out of these processes the first, the dehydration of lipid bilayers, is the rate-limiting step in SNARE-assisted membrane fusion. The time until the hydration barrier is crossed depends on the applied force, whereas the time from the stalk intermediate to hemifusion, consecutive full fusion, and one-step full fusion is almost independent of external load.

The simplest way to describe the reaction rate k of a system under external force F is provided by Bell's theory (23): $k(F) = k_0 \exp(\beta x^{\ddagger} F)$ with the zero force rate $k_0 = \nu \exp(-\beta \Delta G^{\ddagger})$, the attempt frequency ν, $\beta^{-1} = k_B T$, the height of the energy barrier $\Delta G^{\ddagger}$, and the distance to

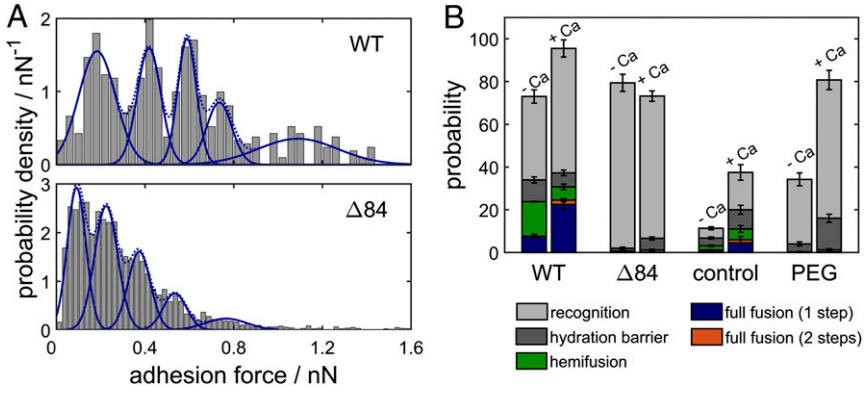

Fig. 3. (*A*) Histogram of adhesion forces obtained from experiments without fusion events for WT SNARE proteins (*Top*) and the Δ84 mutant (*Bottom*) in the presence of calcium ions. Between one and five SNARE complexes are formed, each contributing an adhesive force of 200 pN in case of the WT and only 120 pN for the mutant. (*B*) Probability that the indicated intermediate is reached at the end of the time trace during a force-clamp cycle for WT SNARE proteins, the Δ84 syb mutant, in the absence of proteins and with the addition of PEG-8000, all with and without calcium ions, respectively. Recognition refers to curves showing no fusion but significant adhesion forces (more than 50 pN). Error bars indicate the SEM.

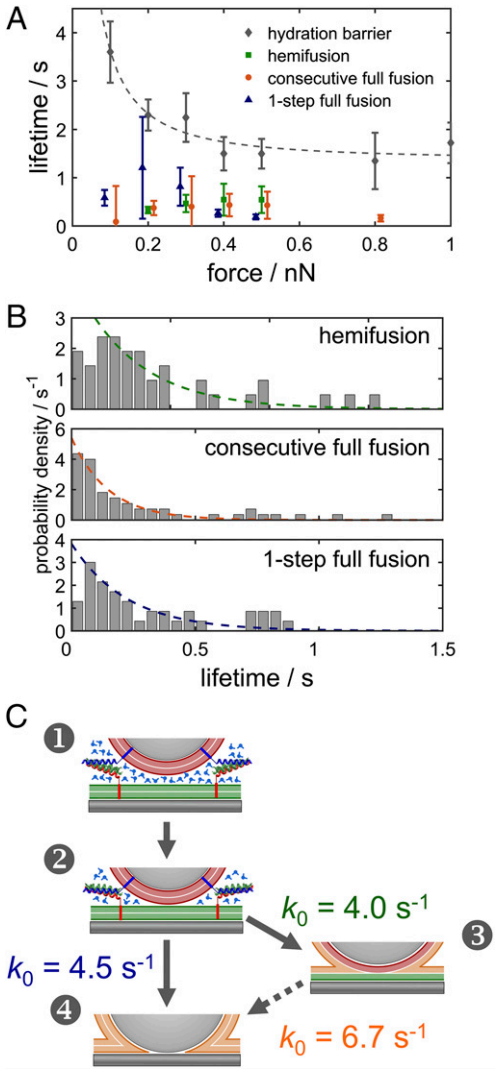

Fig. 4. (*A*) Mean time from initial contact of the two membranes until crossing of the hydration barrier (gray), between dehydration and hemifusion (green), or one-step full fusion (blue) and between hemifusion and consecutive full fusion (orange) as a function of applied force. Error bars indicate the SEM. (*B*) Histograms of the lifetimes of the three respective fusion intermediates fitted with a monoexponential decay. (*C*) Illustration of the fusion pathways found in our experiments.

the energy barrier $x^{\ddagger}$. In our case we need to additionally consider that the contact area A of a sphere and a planar substrate depends on the applied force as described by Hertzian contact mechanics, $A=\pi(3FR/(4E^{*}))^{2/3}$, with the reduced Young's modulus $E^{*}=1/((1-\nu_1^2)/E_1+(1-\nu_2^2)/E_2)$ assuming a bilayer's Young's modulus of $E_1=E_2=20$ MPa (24), a Poisson's ratio of $\nu_1=\nu_2=0.5$, and a probe radius of $R=7.5$ μm. This increase in contact area has two consequences. First, the applied force is distributed over a bigger area, which can be taken into consideration by replacing the force in Bell's theory with the fraction of the loading force acting on the transition state $FA^{\ddagger}/A(F)$, in which $A^{\ddagger}$ denotes the size of the transition state. Butt and Franz (31) devised a similar model to describe the mechanical instability of molecularly thin layers subject to force. Second, the number of lipids in the contact zone increases with force, thereby raising the probability of lipid splaying, the proposed transition state toward solvent-free bilayer contact (32). Therefore, the zero force rate $k_0=N_L/\tau_L$ scales linearly with the number of lipids $N_L=A/A_L$ in the contact zone calculated from the contact area A and the area per lipid $A_L=0.7$ nm^2 (33). $k_L=\tau_L^{-1}$ is the reaction rate at zero force for a single lipid.

In addition, we need to add a force-independent time constant τ_{OS} capturing lateral diffusion of opposing SNARE proteins until successful complex formation occurs. Fitting the Bell model considering the area dependency of the contact area and attempt frequency $\tau(F)=1/(k_LN_L)\exp\left(-\beta x^{\ddagger}A^{\ddagger}F/A\right)+\tau_{OS}$ (Fig. 4*A*, dashed line) we obtain $A^{\ddagger}x^{\ddagger}=58$ nm^3, $k_L=1.8\cdot10^{-5}$ s^{-1}, and $\tau_{OS}=1.4$ s.

The lifetimes of the other three intermediates were found to depend only weakly on external load (Fig. 4*A*). To extract kinetic information, the lifetimes for all loading forces were pooled and fitted with a monoexponential decay, which provides a good description of the experimental data (Fig. 4*B*). The reaction rate toward hemifusion was found to be $k_0=4.0$ s^{-1}, the rate toward consecutive full fusion was $k_0=6.7$ s^{-1}, and the rate of one-step fusion was $k_0=4.5$ s^{-1}. Compared with the rate $k_L=1.8\cdot10^{-5}$ s^{-1} at zero force for crossing of the hydration barrier these subsequent processes are considerably faster.

Discussion

Computational models of membrane fusion describe the merging of two bilayers as a sequence of events initiated by crossing of the hydration barrier to allow solvent-free contact of the two opposing bilayers, followed by widening of a hydrophobic fissure in bilayers. Expansion of the stalk or inverted micelle formation can lead to a hemifusion diaphragm that can progress via pore formation to complete membrane merging (5, 6, 10, 32, 34). Parallel to this canonical description of fusion, there are numerous descriptions of direct transitions from a prefusion stalk directly to a fusion pore (6, 35, 36). Free energy barriers of several tenths of k_BT have been predicted, rendering fusion of membranes without catalysts such as SNARE proteins highly unlikely. The accepted model for SNARE function in fusion is directional N- to C-terminal zippering of a *trans* SNARE complex, thereby pulling opposing membranes together to conquer the hydration barrier (1, 2, 22, 28).

Although computational and theoretical models of membrane fusion are sophisticated and ample, experimental evidence for intermediates of this process is sparse, pathways largely unknown, and free energy estimations unavailable.

Here, we devised a setup that gives access to the free energy barriers and lifetimes of fusion intermediates in the presence of SNAREs by controlling this interbilayer distance through an external load. We build on the seminal work of Moy and coworkers (19) and Israelachvili and coworkers (16, 17), who used the AFM or surface-force apparatus, respectively, to discover fusion events in force distance curves.

Compared with previous work we changed the setup such that it allows us to work in force-clamp conditions to clearly identify intermediate states of fusion and reconstruct the individual fusion trajectories.

In the presence of WT SNAREs we found three intermediate states with an appreciable lifetime assigned to stalk formation, hemifusion, and full fusion. Assignment of hemifusion and full fusion was based on the average step height corresponding to loss of single or double bilayer thickness and correlation with an increase in adhesion forces due a closer distance between the colloidal probe and the planar surface after breakup of intermediate states. Additionally, we observed smaller steps of 1–2 nm occurring most abundantly before hemifusion or full fusion events. These were attributed to crossing of the hydration barrier and resting presumably in a stalk-like intermediate state, because they agree well with the critical distance for stalk formation as predicted from X-ray crystallography (8, 37, 38). This assignment is further supported by an increased number of hydration barrier crossings, when the barrier is lowered by the addition of PEG-8000 and calcium (Fig. 3*B*). Aeffner et al. (8) used X-ray

diffraction of multibilayer stacks to reconstruct stalk structures in protein-free membranes to obtain data on geometry, curvature, and hydration energies. The authors found that dehydration of bilayers is the key step to promote stalk formation, which becomes favorable at a critical interbilayer separation of 0.9 nm and a lateral size of 20 nm^2 (i.e., bilayers fuse as soon as this critical separation has been reached). Knecht and coworkers (32) also report that the initial distance between the membranes is 2–3 nm for lipid bilayer stacks at full hydration, as arising from a balance between short-range repulsion versus long-range van der Waals attraction.

Once the hydration barrier is crossed we identified two distinct pathways toward completely merged bilayers in agreement with computational predictions (6, 35, 36): hemifusion followed by subsequent full fusion and direct full fusion without populating a hemifusion intermediate. The direct pathway to full fusion was observed much more frequently (more than 10 times) compared with the pathway via a hemifusion intermediate. At the same time, the transition from a hemifusion diaphragm toward full fusion occurred very rapidly with a time constant of $\tau = 1/k_0 = 150$ ms. These apparently contradictory results indicate the existence of a second reaction path besides fusion pore opening that is capable of stabilizing the hemifusion intermediate, while being invisible to our deflection readout. A proposed mechanism for stabilization of the hemifusion diaphragm is lateral expansion, which reduces the curvature stress in the diaphragm edge (6, 39). This effect is probably even more pronounced in our special geometry, because both the relatively large probe, with a diameter multiple orders of magnitude larger than a synaptic vesicle, as well as the adhesion of the membranes to the substrates is able to promote expansion of the hemifusion diaphragm.

Apart from changes in lipid topology we also observed docking events due to SNARE recognition. Upon retraction, we identified molecular rupture events associated with individual unzippering of SNARE complexes. We found that replacing WT synaptobrevin with the Δ84 syb mutant arrests the system into a docked state, in accordance with Hernandez et al. (28), who found that the Δ84 syb mutant shows only tight docking as a result of partial complex assembly. This perfectly agrees with our finding that the Δ84 syb mutant displays forces per molecule (100 pN) significantly smaller than those of the WT SNARE (200 pN) but large enough to keep the membranes together. Because most of the free energy stored in SNARE complex formation is dissipated, the incomplete zippering might prevent barrier crossing associated with stalk formation (6).

Calcium increases the probability of full fusion for SNARE-free membranes as well as membranes containing SNAREs (Fig. 3*B*), whereas in the absence of calcium the hemifused state was found more frequently. Furthermore, we found that SNARE zippering in the absence of calcium is incomplete, inferred from the rupture force histograms revealing only ∼70 pN for a single SNARE complex in the absence of calcium in contrast to 200 pN found for SNAREs in the presence of calcium (26, 40–42). Because it is known that SNARE assembly is not affected by calcium (12, 43), we attribute the reduction in rupture force to incomplete zippering of the SNARE complex, in agreement with recent findings of others (11, 14, 15), who found distinct stages of SNARE zippering. As has been predicted by Risselada et al. (39) and recently shown by Hernandez et al. (28), SNARE zippering needs to progress up to the *trans* membrane domain to facilitate full fusion. Therefore, incomplete zippering of the SNARE complex explains the decrease of the probability for full fusion in the absence of calcium. Complete zippering of the opposing SNAREs is presumably prohibited by hydrostatic repulsion between the two bilayers. Additionally, calcium induces a condensation of negatively charged headgroups, in our case PS, leading to asymmetric tension between the two leaflets, which has been shown to facilitate membrane fusion (5). This also explains the increased fusion rate when calcium is added to a SNARE-free system. Jeremic et al. (38) found that the presence of SNAREs decreases the calcium requirement for fusion and also increases the fusion yield. Calcium neutralizes the negatively charged headgroups, resulting in closer distance of the two bilayers allowing the SNAREs to fully zipper, which eventually removes interlamellar water molecules. The observed calcium dependency might be different if highly curved membranes are used as in the case of vesicle studies. Our findings might help to resolve the inconsistent reports about the apparent calcium dependency of SNARE-mediated membrane fusion.

Our experimental approach enables us to obtain lifetime force spectra of fusion processes, offering a rare opportunity to get a glimpse at the rate-limiting steps and energy landscape of membrane fusion. Essentially, we found that in the presence of SNAREs the barrier associated with the process from docking toward a stalk-like intermediate dominates over all other reactions. Schwenen et al. (44) also found that the step from the docked to the intermediate state is rate-limiting by monitoring the residence time of vesicles attached to pore-spanning bilayers (30 s). Note that the overall time scales of the measurements found in this study are smaller because we do not have to wait for lateral diffusion of lipid dyes to detect the steps in cantilever deflection.

Interestingly, we found, that only the first energy barrier toward fusion, the formation of a solvent-free bilayer contact, depends on the applied load. This indicates that the reaction coordinates of the consecutive steps toward fusion might have an orthogonal component to the direction of the force, which is along the normal of the membrane plane. Our result agrees with the fusion mechanisms found in simulations, where fusion is initiated by splaying of a single lipid and followed by lateral expansion of the fusion pore (32, 45). This directly implies an important role of lateral tension for the progression from a stalk intermediate toward full fusion, in agreement with recent findings by Wen et al. (46). Using Bell's theory and taking the force-dependent area increase into account, we found a reaction rate of $\tau_L^{-1} = k_L = 1.8 \cdot 10^{-5}$ s^{-1} per lipid for the first energy barrier associated with crossing of the hydration barrier. Smirnova et al. (32) used coarse-grain simulations to find a single lipid attempt frequency $\nu_L = 5.5 \cdot 10^7$ s for the initial hydrophobic contact between two bilayers. Using the identity $k = \nu \exp(-\beta \Delta G^{\ddagger})$, this would correspond to a hydration energy barrier of $\Delta G^{\ddagger} \approx 30\ k_B T$ in the presence of SNAREs. Comparing this to the protein-free case, where 55 $k_B T$ was found by Aeffner et al. (8) for DOPC/cholesterol (80:20) membranes, the energy barrier is greatly reduced but still appreciable. In the same study Knecht and coworkers (32) reported an attempt frequency of $\nu = 6.25 \cdot 10^6$ s for the initiation of the fusion stalk. We found reaction rates of $k_0 = 4.0$ s^{-1} for the formation of a hemifusion diaphragm and $k_0 = 4.5$ s^{-1} for the transition to fully fused bilayer, both relating to a similar energy barrier of $\Delta G^{\ddagger} \approx 14\ k_B T$. The barriers from the stalk intermediate to either the hemifused intermediate or full fusion are therefore substantially lower than the hydration barrier.

In conclusion, we found that the main energy barrier toward fused lipid bilayers in the presence of SNAREs arises from a prestalk structure, in which the rate-limiting step is the displacement of solvent molecules from the interlamellar contact. Our data suggest that once the hydration barrier is conquered direct full fusion without detour over a hemifusion intermediate state is the principal route toward fully merged lipid bilayers in the presence of SNAREs. It is conceivable that in the native system auxiliary proteins help to keep membranes in such close contact that fusion can immediately proceed upon calcium influx.

Methods

Protein Purification and Liposome Preparation. Proteins were overexpressed and purified as described earlier (22, 28, 47). SUVs (small unilamellar vesicles with average diameter of 50 nm) were prepared by detergent removal as described previously (48) and detailed in *SI Methods*.

Preparation of the Colloidal Probe Cantilever and Solid-Supported Membranes. Colloidal probes were prepared by gluing a borosilicate glass microsphere [Ø = (15 ± 1) μm; Duke Scientific] on a tipless MLCT-C cantilever (Bruker) as described earlier (49). Solid-supported membranes were formed by vesicle spreading in HP150 buffer (20 mM Hepes and 150 mM KCl, pH 7.4). For a more detailed description, see *SI Methods*.

Force–Distance Measurements. Force–distance measurements were carried out with an MFP3D (Asylum Research). The spring constants of the cantilevers were calibrated using the thermal noise method and were found to be in a range of 6–12 pN/nm. All force–distance cycles were operated with a forward velocity of 500 nm/s, a retraction velocity of 1,000 nm/s, a contact time of 10 s, and varying loading forces. The measurements were performed in HP150 buffer or in HP150-Ca buffer (20 mM Hepes, 150 mM KCl, and 1 mM $CaCl_2$, pH 7.4), respectively. For each set of parameters at least 200 force–distance cycles were performed.

ACKNOWLEDGMENTS. The project was funded by the Deutsche Forschungsgemeinschaft through the Goettingen Graduate School for Neurosciences, Biophysics, and Molecular Biosciences Grants GSC 226/2 (to H.W.) and SFB 803 B06 (to R.J.) and B08 (to A.J.).

1. Jahn R, Lang T, Südhof TC (2003) Membrane fusion. *Cell* 112(4):519–533.
2. Chen YA, Scheller RH (2001) SNARE-mediated membrane fusion. *Nat Rev Mol Cell Biol* 2(2):98–106.
3. Rizo J (2012) Cell biology. Staging membrane fusion. *Science* 337(6100):1300–1301.
4. Ryham RJ, Klotz TS, Yao L, Cohen FS (2016) Calculating transition energy barriers and characterizing activation states for steps of fusion. *Biophys J* 110(5):1110–1124.
5. Risselada HJ, Bubnis G, Grubmüller H (2014) Expansion of the fusion stalk and its implication for biological membrane fusion. *Proc Natl Acad Sci USA* 111(30): 11043–11048.
6. Risselada HJ, Grubmüller H (2012) How SNARE molecules mediate membrane fusion: Recent insights from molecular simulations. *Curr Opin Struct Biol* 22(2):187–196.
7. Yoon TY, Okumus B, Zhang F, Shin YK, Ha T (2006) Multiple intermediates in SNARE-induced membrane fusion. *Proc Natl Acad Sci USA* 103(52):19731–19736.
8. Aeffner S, Reusch T, Weinhausen B, Salditt T (2012) Energetics of stalk intermediates in membrane fusion are controlled by lipid composition. *Proc Natl Acad Sci USA* 109(25):E1609–E1618.
9. Li F, et al. (2007) Energetics and dynamics of SNAREpin folding across lipid bilayers. *Nat Struct Mol Biol* 14(10):890–896.
10. Chernomordik LV, Kozlov MM (2011) *Membrane Fusion* (Academic, New York).
11. Gao Y, et al. (2012) Single reconstituted neuronal SNARE complexes zipper in three distinct stages. *Science* 337(6100):1340–1343.
12. Domanska MK, Kiessling V, Stein A, Fasshauer D, Tamm LK (2009) Single vesicle millisecond fusion kinetics reveals number of SNARE complexes optimal for fast SNARE-mediated membrane fusion. *J Biol Chem* 284(46):32158–32166.
13. van den Bogaart G, et al. (2010) One SNARE complex is sufficient for membrane fusion. *Nat Struct Mol Biol* 17(3):358–364.
14. Zorman S, et al. (2014) Common intermediates and kinetics, but different energetics, in the assembly of SNARE proteins. *eLife* 3:e03348.
15. Min D, et al. (2013) Mechanical unzipping and rezipping of a single SNARE complex reveals hysteresis as a force-generating mechanism. *Nat Commun* 4:1705.
16. Helm CA, Israelachvili JN, McGuiggan PM (1992) Role of hydrophobic forces in bilayer adhesion and fusion. *Biochemistry* 31(6):1794–1805.
17. Israelachvili JN, et al. (2010) Recent advances in the surface forces apparatus (SFA) technique. *Rep Prog Phys* 73(3):036601.
18. Lee DW, et al. (2015) Real-time intermembrane force measurements and imaging of lipid domain morphology during hemifusion. *Nat Commun* 6:7238.
19. Abdulreda MH, et al. (2009) Pulling force generated by interacting SNAREs facilitates membrane hemifusion. *Integr Biol (Camb)* 1(4):301–310.
20. Brouwer I, et al. (2015) Direct quantitative detection of Doc2b-induced hemifusion in optically trapped membranes. *Nat Commun* 6:8387.
21. Keidel A, Bartsch TF, Florin EL (2016) Direct observation of intermediate states in model membrane fusion. *Sci Rep* 6:23691.
22. Pobbati AV, Stein A, Fasshauer D (2006) N- to C-terminal SNARE complex assembly promotes rapid membrane fusion. *Science* 313(5787):673–676.
23. Butt H-J, Cappella B, Kappl M (2005) Force measurements with the atomic force microscope: Technique, interpretation and applications. *Surf Sci Rep* 59(1–6):1–152.
24. Picas L, Rico F, Scheuring S (2012) Direct measurement of the mechanical properties of lipid phases in supported bilayers. *Biophys J* 102(1):L01–L03.
25. Savić F, et al. (2016) Geometry of the contact zone between fused membrane-coated beads mimicking cell-cell fusion. *Biophys J* 110(10):2216–2228.
26. Liu W, Parpura V (2009) Single molecule probing of SNARE proteins by atomic force microscopy. *Ann N Y Acad Sci* 1152:113–120.
27. Yersin A, et al. (2003) Interactions between synaptic vesicle fusion proteins explored by atomic force microscopy. *Proc Natl Acad Sci USA* 100(15):8736–8741.
28. Hernandez JM, et al. (2012) Membrane fusion intermediates via directional and full assembly of the SNARE complex. *Science* 336(6088):1581–1584.
29. Haque ME, McIntosh TJ, Lentz BR (2001) Influence of lipid composition on physical properties and peg-mediated fusion of curved and uncurved model membrane vesicles: "Nature's own" fusogenic lipid bilayer. *Biochemistry* 40(14):4340–4348.
30. Milovanovic D, et al. (2015) Hydrophobic mismatch sorts SNARE proteins into distinct membrane domains. *Nat Commun* 6:5984.
31. Butt H-J, Franz V (2002) Rupture of molecular thin films observed in atomic force microscopy. I. Theory. *Phys Rev E Stat Nonlin Soft Matter Phys* 66(3 Pt 1):031601.
32. Smirnova YG, Marrink SJ, Lipowsky R, Knecht V (2010) Solvent-exposed tails as prestalk transition states for membrane fusion at low hydration. *J Am Chem Soc* 132(19): 6710–6718.
33. Marsh D (2013) *Handbook of Lipid Bilayers* (CRC, Boca Raton, FL), 2nd Ed, p 1145.
34. Cohen FS, Melikyan GB (2004) The energetics of membrane fusion from binding, through hemifusion, pore formation, and pore enlargement. *J Membr Biol* 199(1): 1–14.
35. Markvoort AJ, Marrink SJ (2011) Lipid acrobatics in the membrane fusion arena. *Curr Top Membr* 68:259–294.
36. Schick M (2011) Membrane fusion: The emergence of a new paradigm. *J Stat Phys* 142(6):1317–1323.
37. Rand RP, Parsegian VA (1989) Hydration forces between phospholipid bilayers. *Biochim Biophys Acta* 988(3):351–376.
38. Jeremic A, et al. (2004) Calcium drives fusion of SNARE-apposed bilayers. *Cell Biol Int* 28(1):19–31.
39. Risselada HJ, Kutzner C, Grubmüller H (2011) Caught in the act: Visualization of SNARE-mediated fusion events in molecular detail. *ChemBioChem* 12(7):1049–1055.
40. Liu W, et al. (2006) Single molecule mechanical probing of the SNARE protein interactions. *Biophys J* 91(2):744–758.
41. Montana V, Liu W, Mohideen U, Parpura V (2008) Single molecule probing of exocytotic protein interactions using force spectroscopy. *Croat Chem Acta* 81(1):31–40.
42. Liu W, Parpura V (2010) SNAREs: Could they be the answer to an energy landscape riddle in exocytosis? *ScientificWorldJournal* 10:1258–1268.
43. Domanska MK, Kiessling V, Tamm LK (2010) Docking and fast fusion of synaptobrevin vesicles depends on the lipid compositions of the vesicle and the acceptor SNARE complex-containing target membrane. *Biophys J* 99(9):2936–2946.
44. Schwenen LL, et al. (2015) Resolving single membrane fusion events on planar pore-spanning membranes. *Sci Rep* 5:12006.
45. Awasthi N, Hub JS (2016) Simulations of pore formation in lipid membranes: Reaction coordinates, convergence, hysteresis, and finite-size effects. *J Chem Theory Comput* 12(7):3261–3269.
46. Wen PJ, et al. (2016) Actin dynamics provides membrane tension to merge fusing vesicles into the plasma membrane. *Nat Commun* 7:12604.
47. Stein A, Weber G, Wahl MC, Jahn R (2009) Helical extension of the neuronal SNARE complex into the membrane. *Nature* 460(7254):525–528.
48. Hernandez JM, Kreutzberger AJ, Kiessling V, Tamm LK, Jahn R (2014) Variable cooperativity in SNARE-mediated membrane fusion. *Proc Natl Acad Sci USA* 111(33): 12037–12042.
49. Lorenz B, Keller R, Sunnick E, Geil B, Janshoff A (2010) Colloidal probe microscopy of membrane-membrane interactions: From ligand-receptor recognition to fusion events. *Biophys Chem* 150(1-3):54–63.
50. Fiske CH, Subbarow Y (1925) The colorimetric determination of phosphorus. *J Biol Chem* 66(2):375–400.
51. Böttcher C, Pries C, Van Gent C (1961) A rapid and sensitive colorimetric microdetermination of free and bound choline. *Recl Trav Chim Pays Bas* 80(11):1169–1178.